1998

Morphological transformation from galaxy harassment

B Moore

G Lake

N Katz
University of Massachusetts - Amherst

Recommended Citation
Moore, B; Lake, G; and Katz, N, "Morphological transformation from galaxy harassment" (1998). *ASTROPHYSICAL JOURNAL*. 367.
10.1086/305264

Morphological Transformation from Galaxy Harassment

Ben Moore [1], George Lake[2] & Neal Katz[3]

1. Department of Physics, University of Durham, Durham, DH1 3LE, UK

2. Astronomy Department, University of Washington, Seattle, USA

3. Department of Astronomy, University of Massachusetts, Amherst, USA

ABSTRACT

Galaxy morphologies in clusters have undergone a remarkable transition over the past several billion years. Distant clusters at $z \sim 0.4$ are filled with small spiral galaxies, many of which are disturbed and show evidence of multiple bursts of star-formation. This population is absent from nearby clusters where spheroidals comprise the faint end of the luminosity function. Our numerical simulations follow the evolution of disk galaxies in a rich cluster owing to encounters with brighter galaxies and the cluster's tidal field—galaxy harassment. After a bursting transient phase, they undergo a complete morphological transformation from "disks" to"spheroidals". We examine the remnants and find support for our theory in detailed comparisons of the photometry and kinematics of the spheroidal galaxies in clusters. Our model naturally accounts for the intermediate age stellar population seen in these spheroidals as well as the trend in dwarf to giant ratio with cluster richness. The final shapes are typically prolate and are flattened primarily by velocity anisotropy. Their mass to light ratios are in the range 3—8 in good agreement with observations.

Subject headings: galaxies: clusters, galaxies: interactions, galaxies: active galaxies: evolution, galaxies: halos

1. Introduction

The origin of the Hubble sequence (Hubble 1936, Sandage 1961) remains a long standing puzzle in astronomy. Giant galaxies range from ellipticals, slowly-rotating dense

spheroids with little gas, to late–type spirals that are rapidly rotating thin disks of gas and stars. In recent years, two distinct classes of ellipticals have been recognized that are easily separated in plots of nearly any two of their properties, such as central surface brightness versus luminosity (Ferguson and Binggeli 1994, Kormendy 1985). One class includes the bright, giant ellipticals and extends to the rare "dwarf ellipticals" with high surface brightness, M32 being the prototype. The second class consists of low surface brightness spheroidal galaxies that have luminosities $M_B \gtrsim -17$, about 3 magnitudes fainter than L_*, the characteristic break in the luminosity function. (Throughout this paper, all distance dependent quantities assume a Hubble constant of $100h$ km s^{-1}Mpc^{-1}, with $h = 1$.) The dwarf spheroidal galaxies (dSph) in our Local Group of galaxies with magnitudes in the range $-8 \gtrsim M_B \gtrsim -12$ are often considered to be the low luminosity extreme of this sequence, but nearly all other known galaxies in this class reside in clusters (Vader and Sandage 1991). This second class is referred to as "dwarf ellipticals" by Ferguson and Binggeli (1994) and "spheroidals" by Kormendy (1985) who reserves the designation "dwarf ellipticals" for galaxies like M32. After attempting a clumsy hybrid of labels to stay clear of this confusion, we reluctantly follow Kormendy.

There is no shortage of theories for the formation of giant galaxies and the origin of their Hubble sequence. Hoyle (1945) calculated an upper limit to the mass that can radiatively cool and proposed that this imprints a characteristic galaxian mass scale. Gott (1977) and Gunn (1982) promoted two epochs of galaxy formation with ellipticals and bulges forming in an early epoch of Compton cooling and spirals forming by radiative cooling at a later time. This model has faded from popularity because the two formation epochs means that morphological types must arise from fluctuations with vastly different amplitudes, must cool by different physical processes yet have comparable velocity scales and masses.

Most theories for the origin of the Hubble sequence follow Jeans' (1938) assertion that angular momentum is the control parameter. Among the giant galaxies, the Hubble sequence can also be viewed as a mass sequence (Tully, Mould and Aaronson 1982) or virial velocity sequence (Meisels 1983). The larger ellipticals naturally occur in clusters owing to statistical biasing in the hierarchical gravitational collapse model (Bardeen *et al.* 1986), where larger peaks are found to be more strongly clustered than smaller ones. Unfortunately, the variation in the angular momentum of protogalaxies in the hierarchical model is small compared to the observed variation across the Hubble sequence. Furthermore, the angular momentum of halos correlates poorly with any other property such as local overdensity (Barnes and Efstathiou 1987, Ryden 1988).

In order to match the wide variations in the observed properties of galaxies we need a

mechanism that can increase the available stretch and correlations in the hierarchical model. One way to do this is to form elliptical galaxies by the merger of two spirals (Toomre 1977). Despite continuous assertions of its demise (Ostriker 1980, van den Bergh 1982, Carlberg 1986), it seems fairly robust (Lake and Dressler 1986, Lake 1989, Zepf and Ashman 1993). However, ellipticals are generally found within larger structures with collapse times that are shorter than the cooling time required to make a disk. Lake & Carlberg (1988ab) and Katz (1991) found that the Hubble sequence could also arise if the relative amplitude of small scale fluctuations increased with mass or binding energy. If larger mass fluctuations have greater small scale power, then their lumps lead to a transfer of angular momentum from the luminous material to the dark matter. An elliptical galaxy easily results from a lumpy collapse model without disks having already formed. Similarly, Lake & Carlberg noted that small scale power must be suppressed in order for a disk to survive, an effect that was reexamined by Toth and Ostriker (1992).

Spheroidal formation theories have a shorter history and have focused on incremental changes to the giant galaxy theory. The popular model of Dekel and Silk (1986) combines the notion of lower amplitude peaks in the hierarchical model with the use of stellar winds or supernovae to reshape the small galaxies that have low binding energy by expelling their gas (Larson 1974, Vader 1986). There are many problems with this scenario, *e.g.* the clustering properties of dwarfs is opposite to the expectations of the Dekel and Silk model (Ferguson and Binggeli 1994). The model also has the seemingly impossible chore of explaining the general properties of both rapidly-rotating gas-rich dwarfs and gas free dwarf spheroidals.

Recent Hubble Space Telescope (HST) observations (Dressler *et al.* 1994a) have revealed that the morphologies of galaxies in clusters have changed dramatically since $z \sim 0.4$. Over 20 years ago, Butcher and Oemler (1978, 1984) discovered a large population of "blue galaxies" in clusters at $z \sim 0.4$. The HST frames show that at $z \sim 0.4$, the giant ellipticals are already in place, but the ubiquitous "blue galaxies" are distorted spirals that have vanished from clusters at the present epoch (Dressler *et al.* 1994a). The population difference is greatest at lower luminosities; 90% of galaxies fainter than $L_*/5$ in distant clusters are bulgeless "Sd" disk systems, whereas 90% are spheroidals in nearby clusters such as Virgo or Coma (Sandage *et al.* 1985, Thompson and Gregory 1993). Couch *et al.* (1994) present spectroscopic evidence that the distorted blue galaxies at $z \sim 0.3$ have undergone multiple burst events separated by 1–2 Gyr.

In hierarchical clustering models, the influx of field galaxies into clusters peaks at $z \sim 0.4$ (Kauffmann 1995). A complete picture emerges of both the Butcher–Oemler effect and the morphological transformation if we can identify a mechanism that begins

when spiral galaxies enter clusters, causes a few episodes of distortion and star formation within each galaxy over an interval of 1–2 Gyr and ultimately turns the dwarf spirals into spheroidals in 4–5 Gyr.

Several possible mechanisms have been proposed for the Butcher–Oemler effect: mergers (Icke 1985, Miller 1988), gas compression in the cluster environment (Dressler and Gunn 1983) and tidal compression by the cluster (Byrd and Valtonen 1990, Valluri 1993). Nearly all of these mechanisms can make starbursts, but they all fail other critical tests (c.f. Valluri and Jog 1993). Merging is a one time event in contrast to the spectroscopic evidence of multiple bursts found by Couch *et al.* (1994). From their HST images, Oemler *et al.* (1996) conclude that merging is implausible as the blue galaxy fraction is large and the merging probability is low. They also observe disturbed spirals throughout the cluster, whereas both ram pressure stripping and global tides only operate efficiently near the cluster's center. Furthermore, Valluri and Jog (1993) have shown that the observed relationship between HI deficiency and size is exactly opposite to that expected from ram pressure or evaporative models. Finally, there is no correlation between the spiral fraction and X-ray luminosity of clusters. None of the other models for the Butcher–Oemler effect discussed above address the issue of present day remnants: how are the ubiquitous small spheroidals created as the distorted spirals disappear?

Recently, we proposed a new mechanism for the Butcher–Oemler effect in clusters—"galaxy harassment" (Moore *et al.* 1996). At speeds of several thousand kilometers per second, close encounters with bright galaxies cause impulsive gravitational shocks that can severely damage the fragile disks of Sc–Sd galaxies. We will show that these collisions are frequent enough that harrasment occurs throughout the cluster.

Moore *et al.* (1996) used numerical simulations to compare harassed galaxies to HST frames of galaxies in clusters at $z \gtrsim 0.3$. They stated that the cumulative effect of such encounters changes a disk galaxy into a spheroidal galaxy, thus identifying the present-day remnants of the disturbed blue galaxies and explaining the change in galaxy morphologies in clusters since $z \sim 0.4$. In this paper, we provide detailed comparisons of the harassed remnants of late type spirals with the photometric and kinematical properties of dwarf spheroidal galaxies.

2. Simulations of galaxy harassment

We use N-body simulations with only gravitational forces as well as gas dynamical simulations using TREESPH (Hernquist and Katz 1989, Katz, Weinberg and Hernquist

1996) to follow the evolution of "high resolution" model spiral galaxies as they orbit within a rich galaxy cluster.

The cluster model is based on Coma. Its one dimensional velocity dispersion is $\sigma_c = 1,000$ km s^{-1} and the mass within the virial radius (1.5 Mpc) is $7 \times 10^{14} M_\odot$. For an M/L of 250, the total cluster luminosity within this radius is $2.8 \times 10^{12} L_\odot$. The other galaxies in the cluster are drawn from a Schechter (1976) luminosity function parameterized using $\alpha = -1.25$ and $M_* = -19.7$ including all galaxies brighter than $2.8 \times 10^8 L_\odot$ ($H_o = 100$ km s^{-1}Mpc^{-1} and $\Omega = 1$ throughout this paper). This produces a model cluster that has 950 galaxies brighter than the Magellanic clouds, but only 31 brighter than L_*.

The masses and tidal radii of the other galaxies are determined by taking an isothermal model with a dispersion given by the Faber-Jackson relation and tidally limiting it at the galaxy's pericentric distance. They are then modeled by spheres with a softening length equal to half of their tidal radius. Most simulations have no "interpenetrating" collisions. However, any such collision will be more gentle than a collision with a realistic model of a galaxy that is more centrally concentrated. White and Rees (1978) speculated that the dark halos were stripped from galaxies within clusters; we find that the dominant stripping mechanisms are tides and high speed encounters—"galaxy harassment" (Moore, Katz and Lake 1996; hereafter MKL). If galaxies are initially tidally limited by the cluster potential, bright galaxies retain more than half of their mass when followed for 5 Gyr. For greater self-consistency, we reduced the mass of each perturber by 25%, the average loss over a Hubble time (MKL). We left the tidal/softening radius fixed. In the accompanying video, the perturbing galaxies are shown as green dots located at their centers.

The mean ratio of a perturbing galaxy's apocenter to its pericenter in our cluster model is roughly 6-to-1 (this ratio is even larger in infinitie isothermal spheres with isotropic velocities); a galaxy found at a radius of 450 kpc will have a mean orbital radius of 400 kpc and a typical pericenter (r_{peri}) that is slightly greater than 150 kpc. We assign galaxies masses of $2.8 \times 10^{11} (r_{peri}/150\text{kpc})(L/L_*)^{3/4} M_\odot$ corresponding to mass-to-light ratios, $M/L = 26h^2 (r_{peri}/150\text{kpc})(L/L_*)^{-1/4}$. The luminous parts of elliptical galaxies have mass-to-light ratios of $12hM_\odot/L_\odot$ (van der Marel 1991), so our perturbing galaxies have very modest dark halos.

The fraction of the cluster's density attached to galaxies varies with radius from zero at the center to nearly unity at the virial radius. It is ∼20% at the mean orbital radius of our simulated galaxies. The rest of the cluster mass is in a smoothly distributed background represented by a fixed analytic potential. Further details of the cluster model can be found in MKL.

The simulations were originally performed to follow the morphological evolution of galaxies in clusters (Moore *et al.* 1996, MKL), so the parameters were chosen to be typical of the disturbed galaxies seen by HST at redshifts of ~ 0.3. Since we are examining the assertion that the remnants become the spheroidals seen in present-day clusters, we must compare the remnants in our simulations to the brighter spheroidals observed in clusters.

We simulated a number of galaxies with circular velocities of 160 km s^{-1} and 110 km s^{-1}. Using the Fisher–Tully (1981) relation, the luminosity of a galaxy with a circular velocity, $v_{circ} = 160$ km s^{-1} is $\sim L_*/5$, while the $v_{circ} = 110$ km s^{-1} would correspond to $\sim L_*/20$. The $L_*/5$ model galaxies have exponential disks with scalelengths of 2.5 kpc and scaleheights of 200 pc. The $\sim L_*/20$ models had disk masses that were half of the $L_*/5$ models and scalelengths of 2 kpc, giving an initial disk surface density about 20% lower than the larger models. They were all constructed with a Toomre (1964) "stability" parameter $Q = 1.5$ and run in isolation for 2 Gyr before being set into orbit in the cluster. Gas disks were only used in the larger galaxies and were started with particles on cold circular orbits.

The dark halo of each galaxy is spherical and isothermal with a core radius of $(v_{circ}/160 \text{ km s}^{-1})^2$ kpc and is tidally truncated at the pericenter of the galaxy's orbit within the cluster. At 4 disk scalelengths (10 kpc) the initial ratio of dark matter to stars to gas is 11:4:1 in the $L_*/5$ models. At 8 disk scalelengths (20 kpc), the ratios are 20:5:1 and the total mass is $\sim 10^{11}(v_{circ}/160 \text{ km s}^{-1})^3 \text{M}_\odot$. We fixed the mean radius of the orbits at 450 kpc as a representative value that prevented the dimensionality of the parameter space from getting out of control.

The gas was treated using smoothed particle hydrodynamics that models the effects of shocks and cooling assuming using primordial element abundances. The simulations with gas have no prescription for star formation, representing an extreme case. To explore the opposite extreme, we also ran simulations without gas to represent the case where the gas forms stars the first time it is disturbed. The 15 models that were run are all tabulated in Table 1. These models were run in a variety of ways: 1) with and without gas included (the combined mass of the stellar and gaseous disk is fixed), 2) with and without the perturbing influence of other cluster galaxies and 3) on circular and elliptical orbits.

Of the 15 simulations shown in Table 1, models 1–10 and 11–15 have $v_{circ} = 160$ km s^{-1} and $v_{circ} = 110$ km s^{-1} respectively. Apart from the initial conditions of the two separate models, all the quantities are measured after 3–5 billion years of evolution in the cluster. (The runs with gas were stopped when the central gas density became so large that the required timestep became prohibitively small.)

We have intentionally made some conservative assumptions to ensure that our results are robust. For a model galaxy on a fixed orbit, the havoc wreaked by harassment depends on the square of the masses of the largest galaxies encountered. The most massive galaxies are giant ellipticals that are far less prone to harassment owing to their high internal densities, yet we have reduced the masses of all galaxies by the same time averaged value of 25%. At a fixed mean orbital radius, galaxies on elongated orbits experience greater harassment. We follow galaxies that have apo/peri ratios of 2 (*i.e.* apocenter at 600 kpc, pericenter at 300 kpc), whereas the typical value is ~ 6. As a result, our model galaxies avoid extremes of the cluster distribution and start with large dark halo masses determined by the tidal limit at their atypically large pericenters. Both effects serve to underestimate the effects of harassment.

In MKL we examined the evolution of spherical systems owing to the individual and combined actions of tides and collisions with other galaxies. We noted the transformation of small disk galaxies into spheroids when we proposed that harassment causes the Butcher–Oemler effect (Moore *et al.* 1996). Here, we present detailed photometric and kinematic properties of the harassed remnants and compare to spheroidals in clusters.

The evolution proceeds in a violent, chaotic fashion that is best appreciated by watching the accompanying video. The first sequence shows the orbiting galaxy and the entire simulated cluster. It may appear that global cluster tides are stripping most of the material from the model, but it is the collisional shocks from other galaxies that drives the bulk of the dark matter over the tidal radius (a model galaxy on the same orbit but with no perturbers looses a great deal less mass). The stripped material continues to follow the orbital path of the galaxy and is seen as the prominent tidal tails. The third dynamical sequence (the stellar distribution framed in an 18 kpc box) shows the transformation from disk to spheroidal. The first encounters lead to a bar-like phase that is rapidly heated into a more prolate configuration. As the stars and gas lose angular momentum to the dark halo and perturbing galaxies, it becomes harder to physically remove material from the galaxy.

This strong evolution of galaxies in clusters has seemed counterintuitive to many of our colleagues prompting us to remark on "harassment" in the broader context of collisional dynamics. In most stellar systems, the first sign of encounters is "relaxation"—the redistribution of orbital velocities leading to a Maxwellian distribution. The relaxation time in a cluster of galaxies is 100 times their lifetime. However, the binding energy of a small spiral galaxy is $\lesssim 10^{-2}$ of its orbital energy and $\lesssim 10^{-3}$ of the orbital energy of an L_* galaxy. Internal energy transfers via galaxy-galaxy interactions provides an important internal heating source with a timescale that is much shorter than the relaxation time. These circumstances are clearly unique when we contrast them to other astrophysical

environments where encounters occur, *e.g.* close stellar encounters in star clusters (Press and Teukolsky 1977) or the interaction between a proto-stellar disk and passing stars (Ostriker 1994). In the former case, the orbital kinetic energy is much less than the stellar binding energy, whereas in the latter case the internal and orbital energies are comparable. These cases lead to an intuition about the timescales of "relaxation" versus internal heating in stellar systems that is clearly false for small galaxies in clusters.

3. The properties of harassed disk galaxies

Table 1 displays a variety of data for the final states of the remnants. Models 1 through 10 are the larger disks and 11 through 15 are the smaller ones. Column 2 states whether other galaxies were included as perturbers within the cluster (the alternative being a completely smooth cluster potential). The apocluster and pericluster radii of the initial disk's orbit are given in column 3. Columns 4—7 are the final masses of the remnants: the fraction of stars that remain bound to the final remnant $M_{*,f}/M_{*,i}$, the total mass of the stars in the remnant in solar units $M_{*,f}/M_{\odot}$, the total mass of dark matter within the tidal radius of the final remnant in solar units $M_{d,f}/M_{\odot}$ and the ratio of total mass to the disk mass inside the half-light radius of the remnant $M_{T,f}/M_{*,f}$. Column 8 is the tidal radius of the remnant fit from the final density profile of dark matter r_t while column 9 is the effective radius defined by the projected radius containing half of the light r_e. Column 10 is the mean column density of stars within r_e. The three components of the velocity ellipsoid σ_x, σ_y and σ_z are shown in column 11. Column 12 gives the rotation velocity about the the three axes nx, n_y and v. The last two columns define the shape of the three dimension figure, measured at $2r_e$ using the ratio of the short to long axis c/a and the intermediate to long axis b/a. If $c/a \sim b/a$, the object is nearly prolate. If $b/c \sim 1$, then it is oblate.

3.1. Evolution of the mass distribution

The dark halos were constructed out to the tidal radius defined by the cluster potential at the galaxy's pericentric distance. In the comparison runs without other perturbing galaxies, we find that some of the dark halo is stripped owing to tidal shocks at pericenter, but the simulations with perturbers demonstrate that far more mass is lost owing to encounters with perturbing galaxies. At the start, model galaxies are dark matter

dominated beyond about 2 disk scalelengths. After several billion years of evolution and heating, they are frequently baryon-dominated at all radii. At a fixed radius in the galaxy, more dark matter can be lost than stars because of the orbital distribution of the two components. The dark matter is on eccentric orbits that reach the tidal radius while disk material on circular orbits remains safely bound. This evolution is shown in Figure 1(a) where we plot the contribution to the effective rotation curve provided by the stars and dark matter separately. Figure 1(b) shows similar results but for one of the simulations with gas.

Figure 2 shows the initial and final mass distributions of the separate components: stars, gas, dark matter and the combined total. We find that 25–75% of the stars are stripped over about 5 Gyrs. When we include a gaseous disk, the stellar mass loss drops significantly owing to the central density increase. We emphasize the importance of the inner mass distribution in determining the evolution of the system. If the central mass distribution can respond adiabatically to the perturbation then the visible effects of harassment in our simulations are considerably weaker. However, we have not included a recipe for star formation so it is unclear how sensitive the star-formation rate is to tidal perturbations.

3.2. Luminosity profiles

Figure 3(a) shows the time evolution of the stellar density as the model galaxy moves on a circular orbit at 450 kpc without any perturbing galaxies. After 5 Gyrs of evolution, neither the density plot nor visual inspection shows much change. In Figure 3(b), the same model galaxy is on an eccentric orbit with apocenter:pericenter of 600:300 kpc, again without any pertubing galaxies. The first pericentric passage causes a bar instability followed by an increase in the inner stellar density. The outer stellar density profile doesn't show much change. Figure 3(c) is the same high resolution galaxy model as Figure 3(b) but includes the other cluster galaxies as perturbers. Now, the stellar density steepens significantly beyond ∼kpc as mass is stripped from the outer disk.

If we follow a gaseous component then the stellar density profile evolves more strongly in the central region, but less strongly beyond a few kpc. The gas collapses with the stars into a bar configuration, but continues to cool and sink as it looses energy via radiation and angular momentum loss to the stars and dark halo. The contraction of the gas causes an adiabatic contraction of the stellar distribution, leading to a power-law luminosity profile down to our resolution limit. The increase in binding energy due to the change in central

density makes it harder for perturbations to strip stars from the galaxy. As a result, the outer luminosity profile evolves less strongly than in the simulations without gas – see Figure 3(d). We note here that the luminosity profiles are strongly affected by the presence of a dissipative component. The inclusion of star formation and feedback would likely halt the collapse of the gas and resulting profile would lie between the two extreme cases that we examined.

Binggeli and Cameron (1991) provide luminosity profiles for several hundred spheroidal and nucleated dwarfs (dE and dE,N respectively in their notation). Most bright spheroidals show an inner extended excess of luminosity over a King (1966) model ($\sim$ 1 arcsecond $\equiv$ 100 pc at the distance of the Virgo cluster). The latter class are distinguished by an additional "stellar-like" nulceus. Most spheroidals fainter than $M_{_B} \sim -16$ show no excess.

Figure 4 shows the surface brightness profiles of the harassed remnants. Our simulations were not designed to probe the inner 200 pc, but we do see a clear difference between our simulations that have gas and those that do not. We ran models that had identical mass distributions and orbits with and without gas. The global evolution from a disk to a spheroid is comparable, but the inner density profiles change. In the "no gas" case (dashed–dot line in Figure 4), the remnants are spheroids without a large central luminosity excess. In the models "with gas" (dashed line in Figure 4), the torques of collisions together with the cooling causes the gas to sink and form a density excess similar to the luminosity spike in the nucleated bright spheroidals (Binggeli and Cameron 1991). Even without gas, the profile often becomes steeper and the central density increases compared to the initial disk. This is not caused by two body relaxation; the relaxation times in our simulation are far too long. (This was checked by verifying that the stellar phase densities are not increasing.) Some of our harassed remnants resemble dS0 systems, the lenticular class arising from the survival of a thick stellar disk (Sandage & Binggeli 1984).

3.3. Flattening

The shapes of harassed remnants become progressively rounder as the heating continues. After about 5 billion years of evolution within the cluster the remnants without gas have shapes between E3 to E5, e.g. somewhat flatter than the E3 shape that is the mean for giant ellipticals. The inclusion of gas tends to make the final shapes less eccentric as the ensuing central concentration causes a rounder potential in the inner parts. The increased central density concentration might make it harder to support the box orbits that

are important in maintaining triaxial shapes (Lake and Norman 1983, Gerhard and Binney 1985).

The spheroidals in Virgo show the same trend as they are clearly flatter than normal ellipticals (Ryden and Terndrup 1994). Binggeli and Popescu (1995) separate the nucleated spheroidals and find that they are rounder than the others having flattenings that are similar to giant ellipticals.

With our small exploration of parameter space we cannot study trends in the harassed remnants. However, there are several that one might expect. As the collisional heating progresses, the galaxies should become progressively larger and rounder creating a anti-correlation between surface brightness and flattening.

Figure 5 shows the evolution of the axial ratios in various simulations, owing to the "tidal shocks" at pericentric passage. (There is a slight additional heating of the disk owing to the discreteness of the dark halo model.) Figure 5(a) shows the same galaxy on an eccentric orbit with no perturbers, but with the disk orbiting within (dotted line) and perpendicular (solid line) to the orbital plane of the galaxy within the cluster. The ratio of minor to major axis (c/a) measured at twice the effective radii increases from 0.05 to ∼0.2 over 5 Gyrs and disks that lie in the orbital plane are more strongly affected by the cluster tidal field.

When the other perturbing galaxies are included, the disk heating is substantial and the stellar shape evolves dramatically with time. Figure 5(b) shows the evolution of c/a in 4 separate simulations. The first strong encounter drives a strong bar instability and the subsequent evolution shows a steady increase in axial ratio towards "rounder" shapes. The final c/a values range from 0.25 to 0.75. Again, the inclusion of a gaseous disk slows down the evolution and the stellar configuration becomes less responsive to perturbations as the central density increases (Figure 5(c)).

3.4. Stellar kinematics and shapes

The stellar velocity dispersions of models on eccentric orbits without other perturbing galaxies increases slowly with time as tidal shocks from pericentric passage heat the disk. When perturbers are included the velocity dispersions rise more quickly and tend to level off or even start to decrease slowly with time as increasing mass loss causes the galaxy to swell. These effects are shown in Figure 6 where we plot the evolution of the stellar velocity dispersion.

The flattening of galaxies owes to either rotation or anisotropic pressure. For oblate systems that are flattened by rotation, there is a simple relationship between the observed flattening and v/σ the ratio of the rotation velocity to the line-of-sight dispersion (Binney 1978) shown as a solid line in Figure 7. Lake (1983) introduced the parameter $(v/\sigma)^*$, the ratio of the observed v/σ to that required to produce the observed flattening. In giant ellipticals, $(v/\sigma)^* \lesssim 0.3$, while bulges and compact dwarf ellipticals like M32 are flattened by rotation, e.g. $(v/\sigma)^* \sim 1$ (Lake 1983, Davies *et al.* 1983). There are very few spheroidal galaxies with kinematical data, but the sample of six compiled by Ferguson and Binggeli (1994) all have significant velocity anisotropy with $(v/\sigma)^* \lesssim 0.4$. They are clearly not following the trend shown for dwarf ellipticals, but their flattening may owe slightly more to rotation than seen in the giant ellipticals.

The harassed remnants are triaxial ranging from nearly prolate to nearly oblate – see Figure 7. In all cases, the shortest axis is the rotational axis. This leads to a variety of interesting kinematical tests (Binney 1985). When viewed down the intermediate axis, they show the maximum amount of rotation and flattening (c/a and $(v/\sigma)_{max}$ in Table 1). When viewed down the long axis, they appear rounder with nearly the same value of v/σ and the maximum value of $(v/\sigma)^*$ (b/a, $(v/\sigma)_{max}$, and $(v/\sigma)^*_{max}$ in Table 1). Finally when viewed down the short or rotation axis, they show a flattening equal to the ratio of the intermediate axis to the long axis (b/c in Table 1) and $(v/\sigma)^* \sim 0$. It is difficult to compare the complicated distribution derived by sighting through arbitrary viewing angles with a sample of six observed galaxies, but the observed trend of more rotation than giant ellipticals but less than needed for rotational flattening is certainly true for our remnants.

3.5. The fundamental plane

In the multivariate space of galaxy properties (luminosity, size, surface brightness, velocity dispersion, line strengths), galaxies are observed to have highly correlated properties such that they populate a "fundamental plane" (Djorgovski and Davis 1987). Extremely tight correlations exist for elliptical galaxies and bulges that link them as a single family. Spiral disks show their own distinct correlations. The data on spheroidals is sparse owing to the difficulty of measuring the internal kinematics of such faint low surface brightness galaxies. There are some data between $-15 \gtrsim M_B \gtrsim -17$ with a large scatter. To define a plane, these data are "connected" to the observations of the dSphs ($-8 \gtrsim M_B \gtrsim -11$) leaving a gap of nearly 5 magnitudes in luminosity. A departure from the giant E fundamental plane is clear, although the existence of a separate plane is not (Kormendy 1985, Ferguson and Binggeli 1994).

For normal ellipticals, the tight correlations over 2 decades in luminosity are remarkable given the many and varied ways that galaxies are thought to form and evolve. Our proposal that harassment creates spheroidals leads to qualitative and quantitative statements regarding the region of parameter space they inhabit in projections designed to display a fundamental plane. Since their progenitors are disks, we expect more similarity to disk properties than to ellipticals. As they evolve from disks to spheroids, the central properties typically change by a factor of 2, rather than the orders of magnitude that might be required to reach the plane defined by elliptical galaxies. Since the remnants form by stochastic reshaping and stripping, it would be remarkable if they populated a slender plane. However, survival of the final remant imposes some strong contraints, as one might easily guess from the fragility of the initial disks. From our limited number of simulations we find that the final stellar configurations have half light radii up to 50% smaller than the progenitor and a central surface brightness that is 2—3 times larger. The scatter in surface brightness at a fixed r_e is as large as a factor of 2.

3.6. Stellar populations

Ellipticals have old stellar populations that are well-modeled by a single burst of star-formation (c. f. Bender, Burstein and Faber 1993). Spheroidals have intermediate age populations betraying several prominent episodes of star-formation (Held and Mould 1994). Since ellipticals and spheroidals are both deficient in gas, it's something of a surprise that the least massive systems retained their gas for a late epoch of star-formation. However, this follows naturally from our linkeage of the spheroidals to the galaxies forming stars in clusters at $z \sim 0.4$ where the spectral data imply multiple bursts of star formation (Couch *et al.* 1994, Barger *et al.* 1996). We consider radial gradients in §3.9.

3.7. Luminosity function of spheroids produced by harassment

The bright end turnover of the spheroidal luminosity function occurs at $\gtrsim 4$ magnitudes fainter than M_*, there are exceedingly few that are brighter than 3 magnitudes below M_*. Binggeli *et al.* (1988) note that the faint end of the luminosity function is dominated entirely by spheroidals in clusters, while Sd and Im galaxies are dominant in lower-density environments. They state that differences in the slope at the faint end might be explained

entirely by the variations in the ratio of spheroidals to Sd-Im galaxies. Details of the faint end luminosity function are uncertain owing to the myriad of selection effects that plague the inventory of faint, low surface brightness objects (Ferguson and McGaugh 1994), so we will focus our attention on the break at the bright end.

In our work on the collision and tidal heating of spherical systems (Moore, Katz and Lake 1996), we showed that *harassment has virtually no effect on a system as dense as a giant elliptical galaxy or a spiral bulge.* As a result, only purely disk galaxies can be turned into spheroidals. Hence, the maximum luminosity of a purely disk system that falls into the cluster will determine the maximum brightness of the resulting dSph. The luminosity function of galaxies is strongly type specific and pure disk galaxies (Sc or later) with circular velocities greater than ~ 160 km s^{-1} are exponentially rare (Tully, Mould and Aaronson 1982, Meisels 1983, Binggeli *et al.* 1988). The cutoff for Sd-Im galaxies occurs at roughly 125 km s^{-1}. In terms of magnitudes fainter than M_*, these cutoffs are roughly 1.6 and 2.8 magnitudes respectively.

The fate of our model disks with a circular velocities of 160 km s^{-1} should be representative of the evolution of the brightest purely disk galaxies that enter the cluster. They lose between 25% and 75% of there stars (*i.e.* up to a magnitude) and then presumably fade at least a magnitude as the stellar population ages. Taken together, the break at the bright end of the Sc or Sd-Im luminosity functions should create a comparable break in the spheroidal luminosity function that lies $\sim$4 magnitudes below L_*.

3.8. Mass-to Light Ratios, Connection with the dSph Milky Way Satellites

As we mentioned in §3.4, kinematical data on the spheroids is sparse with large scatter in the properties of the handful of galaxies observed between $-15 \gtrsim M_B \gtrsim -17$. The mass to light ratios of the small sample of cluster spheroids ranges from 2 to 8 (Petersen and Caldwell 1993, adjusted for our adopted Hubble constant). Column 7 of Table 1 shows the ratio of total mass to stellar mass $M_{T,f}/M_{*,f} \sim 1.5 - 2$ within the effective radius r_e. To get a mass-to-light ratio for the remnant, one multiplies the expected M/L for the stellar population by this quantity. For these relatively low metallicity systems, one might expect $M/L_* \sim 3 \pm 1$, leading to global values of $3 < M/L < 8$ for our remnants, in good agreement with the observations.

The only hope of discerning trends in quantities like M/L is to connect the scattered cluster points between $-15 \gtrsim M_B \gtrsim -17$ to the even more broadly scattered points defined

by local dSphs at magnitudes ($-8 \gtrsim M_B \gtrsim -11$). The main conclusion drawn is that the mass-to-light ratio is increasing inversely as a power of luminosity, typically $M/L \propto L^{-0.4}$ owing to the $M/L \gtrsim 30$ of Draco and Ursa Minor (Armandroff, Olszewski and Pryor 1995).

What are we to make of the high M/L values of the dSph galaxies? Could Draco and Ursa Minor be remnants of harassment? Earlier, we stressed that harassment is a collective process, phase space densities of dissipationless material do not increase. Therefore a progenitor Irr galaxy harassed to make Draco or Usra Minor must have high central densities and phase densities of dark matter. Such progenitors may well have existed (Lake 1990a). The extreme dwarf irregular GR8 (Carignan, Beaulieu and Freeman 1990) has a central dark matter density of $\sim 0.1 M_\odot \mathrm{pc}^{-3}$ which is only a factor of two less than what is required in Draco and Ursa Minor (Lake 1990b). GR8 is the only such Irr that has been measured while Draco and Ursa Minor are the most extreme dSph galaxies. Further, GR8 has a galactocentric radius of 1 Mpc, 15 times that of the other two. Despite this gross difference in location and its implications for survival, GR8 is close enough to Draco and Ursa Minor that it's not unreasonable to postulate appropriate Irr progenitors.

If harassment turned dwarf irregulars like GR8 into dSphs like Draco and Ursa Minor, we can scale our cluster simulations and timescales to determine the nature of the harassing perturbers in the early Milky Way. The virial mass and radius of an object scale as $R_{virial} \propto v_{circ}$ and $M_{virial} \propto v_{circ}^3$. Given the Milky Way's circular velocity of 220 km s^{-1}, we infer $M_{MW,virial} = 2 \times 10^{-3} M_{Coma,virial}$ and $R_{MW,virial} = 0.15 R_{Coma,virial} = 220$ kpc. The dSph galaxies have masses of $\gtrsim 10^7$ (Lake 1990b) which is $\sim 10^{-3}$ of the mass of the remnants in Table 1. The galactocentric radii of the Draco and Ursa Minor are 70 kpc or $0.32 R_{MW,virial}$ while the galaxies we simulated had guiding centers of $0.3 R_{Coma,virial}$. A galaxy similar to GR8 would be harassed into something resembling Draco and Ursa Minor in 3 Gyrs if the Milky Way had $N \sim 30$ perturbing lumps with mass $M_{MW,pert} \sim 4 \times 10^8 M_\odot$. More generally, the timescale for harassment of GR8 into a dSph is roughly $\tau \sim 3 Gyr (N/30)^{-1} (M_{MW,pert}/(4 \times 10^8))^{-2}$. Models of the early Milky Way often appeal to substructures of comparable mass and number (Searle and Zinn 1978).

We note that Ursa Minor and Draco are well within the virial radius of the Milky Way while the Dwarf Irregular GR8 is clearly well beyond it. Harrassment would not be able to explain dSphs that were members of the Local Group but clearly not satellites of the Milky Way or M31. At a distance of 230 kpc, Leo I would appear to be the greatest challenge (Zaritsky *et al.* 1989). However, it's observed to move outward with a radial velocity of 178 km s^{-1}, so it could have been closer to us than Ursa Minor and Draco just a billion years ago.

3.9. Correlations with clustercentric radius/density

There are two effects that can cause correlations with clustercentric radius—the dynamics of harassment change with radius and hierarchal clustering can produce inherent differences between the center and outer reaches of the cluster.

Harassment depends on collisional frequency, the strength of individual collisions and the strength of the cluster's tidal field. If the dark halos of galaxies scale with radius as the tidal limit, then the heating rate owing to collisions is independent of cluster radius (the collision rate is proportional to galactic density which scales as R_{clus}^{-2}, but this is balanced by the collisional strength since the tidally limited mass of individual galaxies varies linearly as R_{clus} and the strength of the collision scales with the square of the perturber's mass). In the impulse approximation, the heating rate is even constant for any galaxy that finds itself inside a larger virialized structure—independent of the size of the structure. However, the impulse approximation will clearly break down at large radii since collisions in a rich cluster cease to be impulsive if the impact parameter is greater than $\sim$ 100 kpc. (The impulse approximation breaks down faster if the galaxy is in a smaller virialized structure with lower relative velocities).

The cluster's tidal field becomes exceedingly important at the center. Modeling both a small galaxy and a cluster as an isothermal sphere, we find that the tidal radius R_{tidal} of a galaxy with a dispersion σ_{gal} with pericentric radius r_{peri} in a cluster of dispersion σ_{clus} is given by:

$$R_{tidal} = 5\mathrm{kpc}(\frac{r_{peri}}{100kpc})(\frac{\sigma_{gal}}{50\ \mathrm{km\ s^{-1}}})(\frac{\sigma_{clus}}{1{,}000\ \mathrm{km\ s^{-1}}})^{-1}$$

Recall that a galaxy seen at a distance of r_{now} in a cluster has a typical pericenter of $r_{now}/3$, so the typical object with mean orbital radius of r_{now} will have a mean tidal radius:

$$R_{tidal,mean} = 1.67\mathrm{kpc}(\frac{r_{now}}{100kpc})(\frac{\sigma_{gal}}{50\ \mathrm{km\ s^{-1}}})(\frac{\sigma_{clus}}{1{,}000\ \mathrm{km\ s^{-1}}})^{-1}$$

As a result, the smaller spheroidals will be destroyed in the innermost part of the cluster.

Radial gradients of the spheroidal populations may provide some interesting tests of our model. However, one important effect will be common to all models—independent of how the spheroidals might have formed, global tides will coerce the the lowest density (or surface brightness) objects into the diffuse stellar background. We expect that most observed radial correlations will be projections of the fundamental correlation between density and survivability. For example, Secker (1996) looked for a radial gradient in spheroidal colors in the Coma cluster. He fit a power law to his observed distribution $(B-R) \propto R_{proj}^{0.08\pm0.02}$, but the data is flat except for a point at 2 arcminutes (40 $\mathrm{h^{-1}kpc}$) that

is redder by $\Delta(B-R) \sim 0.1$ than the eight outer points. The detailed scatter of the points in plots makes it appear that the inner bin is deficient in bluer points rather than a shifting of the entire distribution with radius. Secker remarks that there is a strong color-luminosity relationship, but quotes theoretical reasons against luminosity segregation that he felt were so strong that he didn't examine his own data. By contrast, Bernstein *et al.* (1995) clearly see a deficiency of low luminosity galaxies in the inner few arc minutes of this cluster.

Finally, radial gradients in properties can arise from the history of the cluster's hierarchical formation via mergers and accretion. In general, the material at the cluster center is older than the material in the outer regions. Hence, the objects in the cluster center experience harassment at earlier times and for longer durations.

From these general principles, we expect that:

- no pure disk galaxy can survive transformation within about half of the virial radius of a large cluster
- spheroidals with small pericentric radii would be destroyed by tides alone
- the look-back time to when spirals were turned into spheroidals and the diffuse light was liberated from galaxies increases toward the center of the cluster.

This leads to a variety of observable effects:

- only the densest spheroidals survive in the inner parts of the galaxies, creating a paucity of the low luminosity spheroids in the central region as seen by Bernstein *et al.* (1995)
- since survival depends on density, any correlations between density and color/metallicity (including indirect correlations owing to luminosity or binding energy) will create color gradients in the surviving ensemble of spheroidals as seen by Secker (1996)
- there will be an age gradient in the diffuse light with the central regions being older than the inner regions, but color gradients will depend on metallicity and the central diffuse light will also include the "splashes" of cannibalism making specific predictions difficult (the previous "bullet" captures the dominant effect)
- nucleated spheroidals will always be more robust than those without a dense nucleus, therefore the fraction of nucleated spheroids will increase towards the center (*c.f.* van den Bergh (1986) and Binggeli *et al.* (1987))

- the heating is greatest in the center leading to lower surface brightnesses and rounder spheroidal galaxies, but the detailed distribution with radius also depends on the survival of such galaxies
- the selective destruction of non-nucleated spheroidals with small pericentric radii will lead to a central velocity ellipsoid that is deficient in radial orbits causing a dip in the cluster's line-of-site velocity dispersion as measured by the non-nucleated spheroidals
- nucleated spheroidals will show a higher central velocity dispersion than non-nucleated
- spiral disks seen in the central regions of clusters will be caused by projection leading to velocity fields that are not virialised as in the case of the Virgo cluster's "backside infall" (deVaucouleurs 1961, Tonry, Ajhar and Luppino 1990) or exhibiting nearly free expansion as seen in the Coma cluster (Bernstein *et al.* 1994)
- in the outer parts of the clusters, the spirals on radial orbits are transformed faster than those on nearly circular orbits as seen in the analysis of gas rich spirals by Dressler (1986)

3.10. Clustering properties

In the Introduction, we noted that several prior models ran afoul of clustering properties. Is harassment any better? It can clearly explain some of the broad trends. Vader and Sandage (1991) stressed that the spheroidals are the most strongly clustered of all galaxies. Their frequency increases sharply with density of the environment. The Virgo cluster has approximately 5 times as many dwarfs per giant as poor groups and this ratio correlates with the group/cluster velocity dispersion as expected in our model (Ferguson and Sandage 1991). Finally, Binggeli, Tarenghi and Sandage (1990) find that "field spheroidals" are companions to giant field ellipticals. They conclude that their phenomenology would be explained by a mechanism that triggered the transformation of Irr to spheroidals in high density environments, which is exactly what harassment does. We stress that harassment occurs in any virialized environment with significant "lumps" to act as perturbers. This is certainly the case for clusters of galaxies and for all current models of elliptical galaxy formation (§I).

4. Conclusion

We have followed the evolution of small disk galaxies in clusters using realistic simulations of the combined action of rapid encounters with cluster galaxies and global tidal heating—"galaxy harassment". We find that the first shocks create the population of distorted spiral galaxies seen in HST images $z \sim 0.4$ cluster. Over a period of a few Gyr, these galaxies evolve into remnants that have surface density profiles, shapes, kinematics, stellar populations and clustering properties that qualitatively match the spheroidal systems in present-day clusters. The assumptions and parameters of our theory are minimal. It relies only on gravitational interactions with the global cluster potential and other galaxies. The strength of these effects is well determined by the observed properties of the clusters and their brighter members. Non gravitational effects such as ram pressure stripping, wind driven expulsion of gas or other hydrodynamic interactions can speed the timescale for the evolution of the gas, but will not sufficiently alter the stellar disk of the galaxies observed at $z \sim 0.4$. Further, the harassment timescale matches the interval of multiple starbursts that is inferred in clusters at $z \sim 0.4$ (Couch *et al.* 1994). This provides a limit on the magnitude of additional hydrodynamic effects, assuring us that harassment must be the dominant mechanism.

In this paper, we have focused on the remnants. However, it is clear that roughly 50% of the stars escape into the intracluster medium. They do so within debris tidal streams and thin tails that gradually disperse. A study of these low surface brightness features and the general diffuse light in clusters will be the subject of a future paper.

We would like to thank Thomas Quinn for numorous discussions and his help producing *Galaxy Harassment—The Movie*. This research was supported by NASA's High Performance Computing and Communications Earth and Space Sciences Program, Astrophysical Theory Program and Long Term Space Astrophysics Program. Ben Moore is a Royal Society Research Fellow.

References

Armandroff, T. E., Olszewski, E. W. and Pryor, C. 1995, *A.J.*, **110** , 2131.

Bardeen, J.M., Bond, J.R., Kaiser, N. and Szalay, A.S. *Ap.J.*, **304** , 15.

Barger, A.J., Aragon-Salamanca, A., Ellis, R.S., Couch, W.J., Smail, I. & Sharples, R.M. 1996, *M.N.R.A.S.*, *279*, 1.

Barnes, J. 1988, *Ap.J.*, **331**, 699.

Barnes, J. and Efstathiou, G. 1987, *Ap.J.*, **319**, 575.

Bender, R., Burstein, D. and Faber, S. M. 1993, *Ap. J.*, **411**, 153.

Bernstein, G.M., Guhathakurta, P.. Raychaudhury, S.. Giovanelli, R., Haynes, M. P., Herter, T. and Vogt, N. P. 1992 *A.J.*, **107**, 2307.

Bernstein, G.M., Nichol R.C., Tyson J.A., Ulmer M.P. & Wittman D. 1995, *A.J.*, **110**, 1507.

Binggeli, B. and Popescu, C.C. 1995, *Astr. Ap.*, **298**, 63.

Binggeli, B. and Cameron, L.M. 1993, *Astr. Ap. Suppl..*, **98**, 297.

Binggeli, B. and Cameron, L.M. 1991, *Astr. Ap.*, **252**, 27.

Binggeli, B., Sandage, A. and Tammann G.A. 1988, *Ann. Rev. Astr. Ap.*, **26**, 509.

Binggeli B., Tammann, G.A. and Sandage, A. 1987, *A.J.*, **94**, 251.

Binggeli, B., Tarenghi, M. and Sandage, A. 1990, *A.J.*, **228**, 42.

Binney, J. 1978, *M.N.R.A.S.*, **183**, 501.

Binney, J. 1985, *M.N.R.A.S.*, **212**, 767.

Butcher, H. and Oemler, A. 1978, *Ap.J.*, **219**, 18.

Butcher, H. and Oemler, A. 1984, *Ap.J.*, **285**, 426.

Byrd, G. and Valtonen, M. 1990, *Ap.J.*, **350**, 89.

Carlberg, R. G. 1986, *Ap.J.*, **310**, 593.

Carignan, C., Beaulieu, S. and Freeman, K. C. 1990, *Ap.J.*, **332**, L33.

Couch, W.J., Ellis, R.S., Sharples, R. and Smail, I. 1994, *Ap.J.*, **430**, 121.

Davies, R. L, Efstathiou, G., Fall, S. M., Illingworth, G. D. and Schechter, P. 1983, *Ap.J.*, **292**, 371.

Dekel, A. and Silk, J. 1986, *Ap.J.*, **303**, 39.

Djorgovski, G. and Davis, M. 1987, *Ap.J.*, **313**, 59.

Dressler, A 1986, *Ap. J.*, **301**, 35.

Dressler, A. and Gunn, J.E. 1983, *Ap.J.*, **270**, 7.

Dressler, A, Oemler, A., Butcher, H. and Gunn, J.E. 1994a, *Ap.J.*, **430**, 107.

Dressler, A., Oemler, A., Sparks, W.B. and Lucas, R.A. 1994b, *Ap.J.Lett.*, **435**, L23.

Evrard, A.E. 1991, *M.N.R.A.S.*, **248**, 8p.

Faber, S.M. and Jackson, R. 1976, *Ap. J.*, **204**, 668.

Ferguson, H.C. and McGaugh, S. S. 1994 *Ap. J.*, **440**, 470.

Ferguson, H.C. and Sandage, A. 1991, *A.J.*, **101**, 765.

Ferguson, H.C. and Binggeli, B. 1995, *Astr. Ap. Rev.*, **vol. 6**, 67.

Fisher, J. R. and Tully, R. B. 1981, *Ap. J. Suppl.*, **47**, 139.

Gerhard, O. E. and Binney, J. J. 1985, *M.N.R.A.S.*, **216**, 467.

Gott, J. R. III 1977, *Ann. Rev. Astr. Ap.*, **15**, 235.

Griffiths, R.E. *et al.* 1994, *Ap.J.Lett.*, **435**, L19.

Gunn, J.E. 1982, in *Astrophysical Cosmology, Proceedings of the Vatican Study Week on Cosmology and Fundamental Physics*, ed. M.S. Longair, G.V. Coyne and H.A. Bruck, (Vatican City: Pontifcia Academia Scientiarum).

Held, E.V. and Mould, J.R. 1994, *A.J.*, **107**, 1307-19.

Hernquist, L. 1993, *Ap.J.Suppl.*, **86**, 389.

Hoyle, F. 1945, *M.N.R.A.S.*, 105, 288.

Hubble, E. 1936, *The Realm of the Nebulae*, (Oxford: Oxford University).

Icke, V. 1985, *Astr. Ap.*, **144**, 115-23.

Jeans, J. 1938, *Cosmology and Cosmogony*, (Oxford: Oxford University).

Katz, N. 1992, *Ap. J.*, **391**, 502.

Kauffmann, G. 1995, *M.N.R.A.S.*, **274**, 153.

King, I. R. 1966, *A. J.*, **71**, 64.

Kormendy, J. 1985, *Ap.J.*, **295**, 73.

Lake, G. 1983, *Ap. J.*, **264**, 408.

Lake, G. 1989, *A. J.*, **97**, 1312.

Lake, G. 1990a, *Ap. J. Letters*, **356**, L43.

Lake, G. 1990b, *M.N.R.A.S.*, **244**, 701.

Lake, G. and Norman, C. 1983, *Ap. J.*, **270**, 51.

Lake, G. and Dressler, A. 1986, *Ap. J.*, **310**, 605.

Lake, G. and Carlberg, R. G. 1986a, *A.J.*, **96**, 1581.

Lake, G. and Carlberg, R. G. 1986b, *A.J.*, **96**, 1587.

Lake, G., Katz, N. and Moore, B. 1996, *Ap.J.*, this volume.

Larson, R. B. 1974, *M.N.R.A.S.*, **169**, 229.

Meisels, A. 1983, *Astr. Ap.*, **vol. 118**, 21.

Merritt, D. 1985, *Ap.J.*, **289**, 18.

Miller, R.H. 1988, *Comment. Astrophys.*, **13**, 1.

Moore, B., Katz, N. and Lake, G. 1996, *Ap.J.*, **457**, 455 (MKL).

Moore, B., Katz N., Lake G., Dressler, A. and Oemler, A. 1996, *Nature*, **379**, 613.

Oemler, A., Dressler, A. and Butcher, H. R. 1996, *Ap.J.*, submitted.

Ostriker, E.C. 1994, *Ap.J.*, **424**, 292.

Ostriker, J.P. 1980, *Comm. Astr. Ap.*, **8**, 177.

Ostriker, J.P. and Hausman M.A. 1977, *Ap.J.Lett.*, **217**, L125-9.

Peterson, R. C. and Caldwell, N. 1993, *A. J.*, **105**, 1411.

Press, W.H. and Teukolsky, S.A. 1977, *Ap.J.*, **213**, 183.

Richstone, D.O. and Malmuth, E.M. 1983, *Ap.J.*, **268**, 30.

Ryden, B.S. 1988, *Ap.J.*, **329**, 589.

Ryden, B.S. and Terndrup, D.M. 1994, *Ap.J.*, **425**, 43.

Sandage, A. 1961, *The Hubble Atlas of Galaxies*, (Washington D.C.: Carnegie Institution of Washington).

Sandage, A., Binggeli, B. & Tammann, G.A. 1985, *A.J.*, **90**, 1759.

Sandage, A. & Binggeli, B. 1984, *A.J.*, **89**, 919.

Secker, J. 1996, *Ap.J.Lett.*, **469**, L81.

Searle, L. and Zinn, R. 1978, *Ap.J.*, **225**, 357.

Thompson, L.A. and Gregory, S.A. 1993, *A.J.*, **106**, 2197.

Tonry, J. L., Ajhar, E. A. and Luppino, G. A. 1990, *A.J.*, **100**, 1416.

Toth, G. and Ostriker, J. P. 1992, *Ap.J.*, **389**, 5.

Toomre, A. 1964, *Ap.J.*, **139**, 1217.

Toomre, A. 1977, In *The Evolution of Galaxies and Stellar Populations*, ed. B.M. Tinsley and R.B. Larson, p. 401, (New Haven: Yale University Observatory).

Tully, R. B., Mould, J. R. and Aaronson, M. 1982, *Ap.J.*, **257**, 527.

Vader, P. 1991, *Ap.J.*, **305**, 669.

Vader, P. and Sandage, A. 1991, *Ap.J. Letters*, **379**, L1.

Valluri, M. 1993, *Ap.J.*, **408**, 57.

Valluri, M. and Jog, C. J. 1991, *Ap.J.*, **374**, 103.

Vaucouleurs, G. de. 1961, *Ap.J.Suppl.*, **6**, 213.

van den Bergh, S. 1982, *Pub. A. S. P*, **94,459**.

van den Bergh, S. 1986, *A.J.*, **91**, 271

van der Marel, R. P. 1991, *M.N.R.A.S.*, **253**, 710-26.

Zaritsky, D., Olszewski, E. W., Schommer, R. A., Peterson, R. C. and Aaronson, M. 1989, *Ap.J.*, **345**, 759.

Zepf, S. E. and Ashman, K. M., *M.N.R.A.S.*, **264**, 611.

Figure Captions

Figure 1. (a) The dashed curves are the effective circular velocity at a radius r from the mass distribution of the dark matter alone. Likewise the solid curves show the contribution to the effective rotation curve from the stars. These are both plotted for the initial and final states. This model is does not include SPH. (b) As (a) but shows the effect of including a gaseous disk and more time snapshots are plotted.

Figure 2. The effective circular velocities at a radius r from the center of the model galaxy. Each panel shows the contributions to V_c from the separate components, stars, gas, dark matter and total mass. This model is the same that is plotted in 3(b). The solid and dotted curves show the rotation curves at the initial and final times respectively.

Figure 3. The time evolution of the luminosity density as the model galaxies evolve in the "Coma" cluster: (a) A circular orbit at 450 kpc with no perturbers, (b) An eccentric orbit with apocenter:pericenter of 600:300 kpc and no perturbers, (c) As (b) but with perturbers included, (d) As (c) and including a full SPH treatment of a gaseous disk in the harassed galaxy.

Figure 4. The initial surface brightness profile of the Sd galaxy is shown as a solid line. The dashed and dot–dash lines show the projected luminosity profiles of models with and without a gaseous disk after 3 Gyrs of evolution in the cluster with perturbing galaxies.

Figure 5. The time evolution of the axial ratios of the stellar component of various models: c/a is the axis ratio between the long and short axes and b/a is the ratio between the intermediate and short axes, in each case measured at twice the effective radii, r_e. Each panel shows the evolution of several simulations: (a) eccentric orbit with no perturbers. The solid line is a model in which the plane of the disk is not in the orbital plane and the dotted line is a model that orbits in the plane defined by its disk. (b) eccentric orbits of four separate simulations that include perturbers and random disk orientations, (c) eccentric orbit with perturbers and including SPH treatment of the galaxy disk.

Figure 6. Time evolution of the 1-d velocity dispersion of the stars projected along each of the major, minor and intermediate axis of the model: (a) the model galaxy is on an eccentric orbit with no perturbers and the disk rotates out of the orbital plane of the galaxy, (b) as (a) but the disk rotates in a plane defined by the orbit of the galaxy in the cluster, (c) as (a) but including perturbers, (d) as (a) but including perturbers and a gaseous disk. The dashed lines show results from a separate simulation.

Figure 7. The final shapes of the 11 harassment simulations (perturbers included) plotted against v/σ (v is the rotation velocity and σ is the projected velocity dispersion).

Each model is shown by number for 3 projections: viewed down the long axis (squares), intermediate axis (circles) and short axis (numbers only). The projected flattening is measured at $2r_e$. The line shows the theoretical curve for rotationally flattened oblate spheroids.

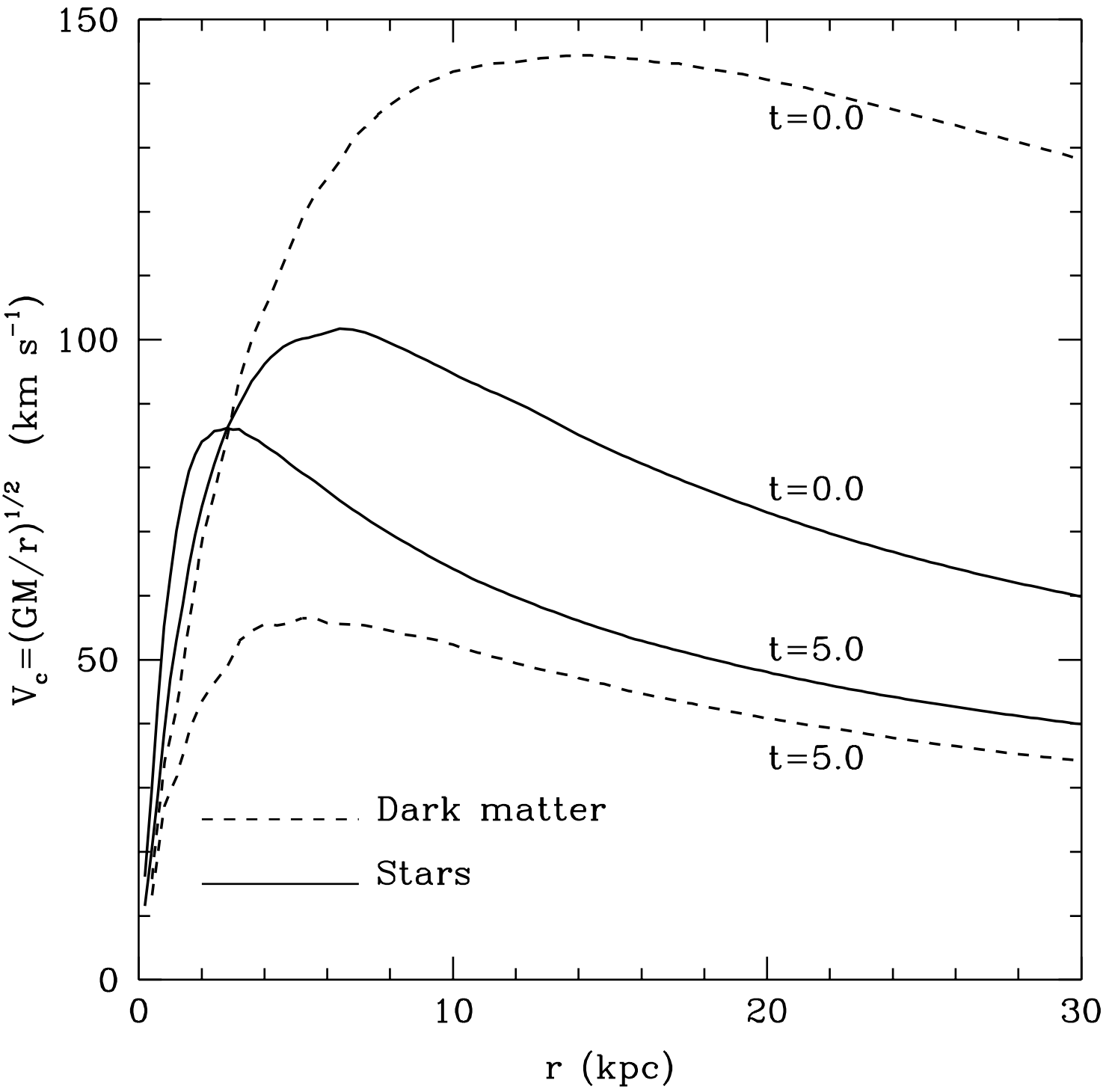
150
100
50
0
0
10
20
30
r (kpc)
$V_c=(GM/r)^{1/2}$ (km s^{-1})
t=0.0
t=0.0
t=5.0
t=5.0
Dark matter
Stars

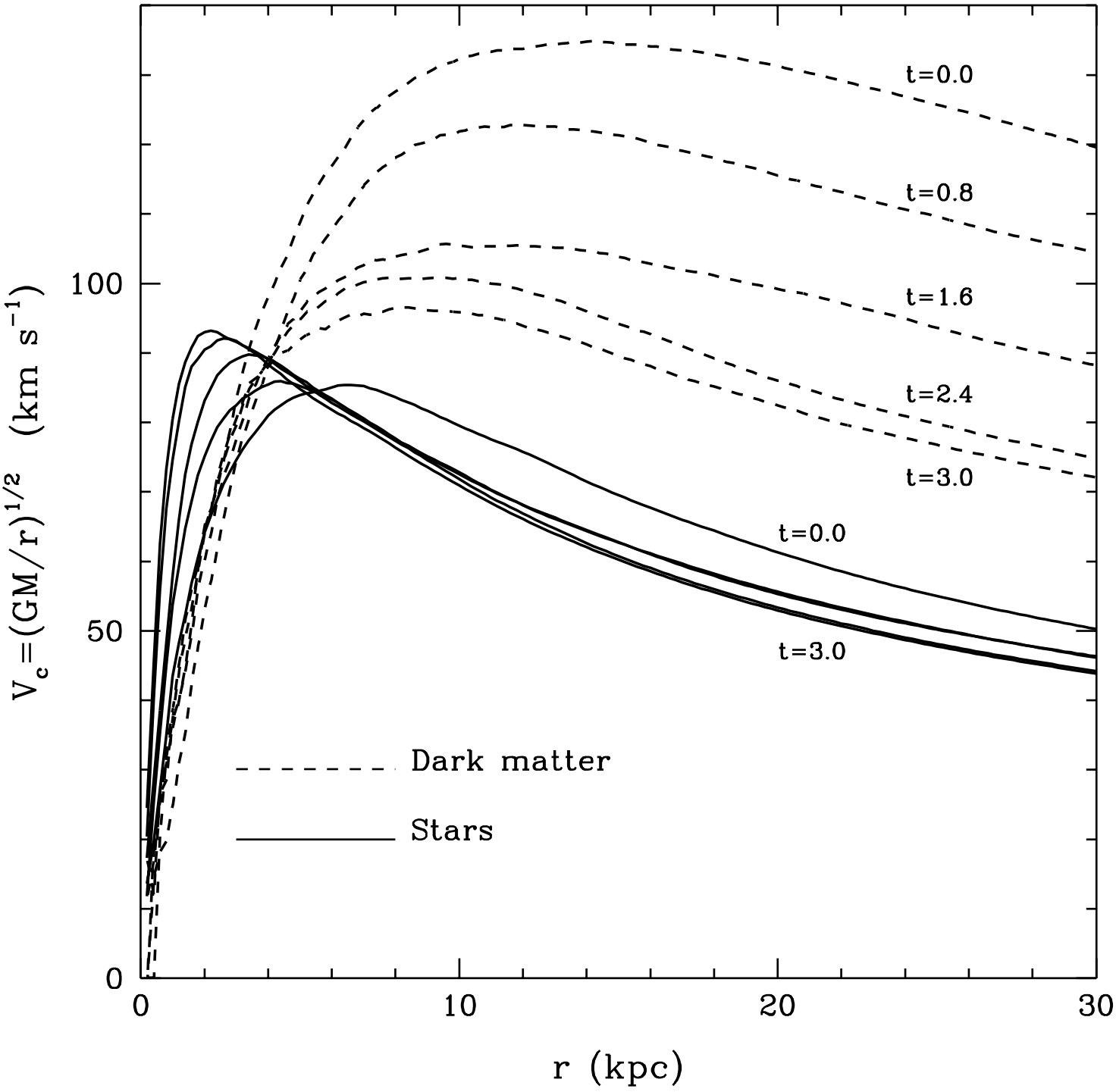
t=0.0
t=0.8
t=1.6
t=2.4
t=3.0
t=0.0
t=3.0
Dark matter
Stars
100
50
0
0
10
20
30
r (kpc)
$V_c=(GM/r)^{1/2}$ (km s^{-1})

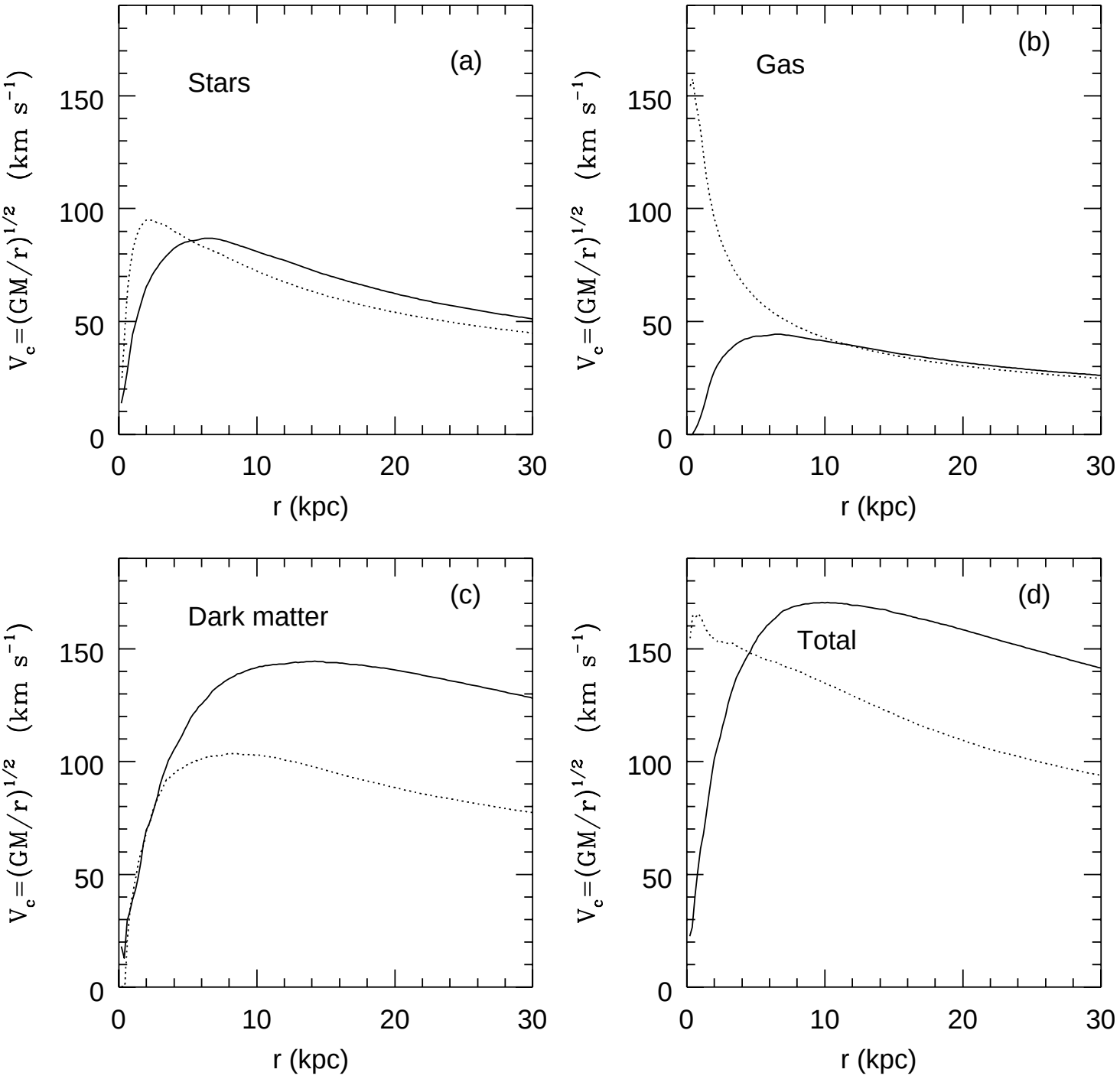
(a)
Stars
(b)
Gas
(c)
Dark matter
(d)
Total
$V_c=(GM/r)^{1/2}$ (km s^{-1})
r (kpc)
0
50
100
150
0
10
20
30

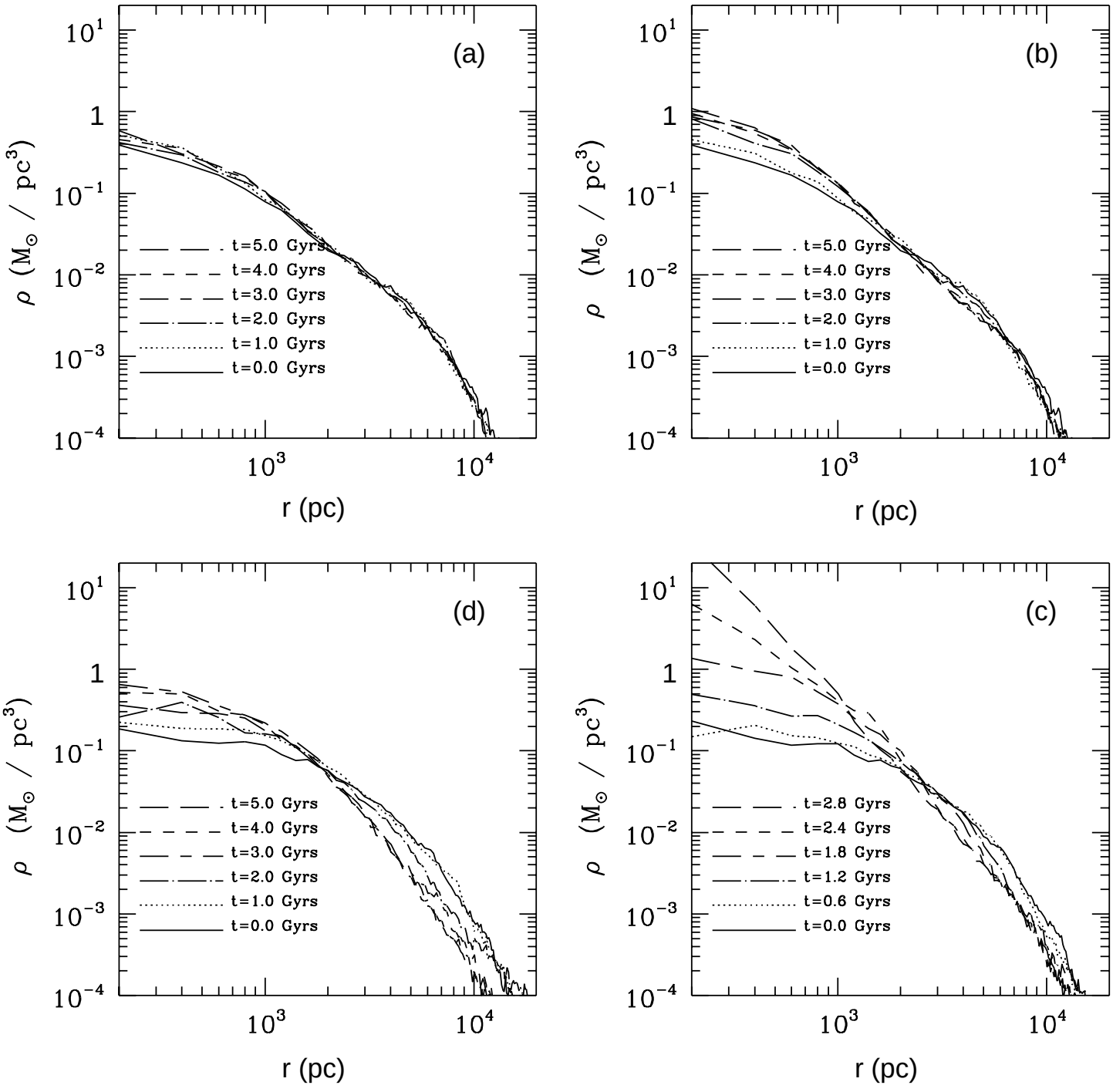
(a)
(b)
(c)
(d)
ρ (M⊙ / pc³)
r (pc)
t=5.0 Gyrs
t=4.0 Gyrs
t=3.0 Gyrs
t=2.0 Gyrs
t=1.0 Gyrs
t=0.0 Gyrs
t=2.8 Gyrs
t=2.4 Gyrs
t=1.8 Gyrs
t=1.2 Gyrs
t=0.6 Gyrs
t=0.0 Gyrs

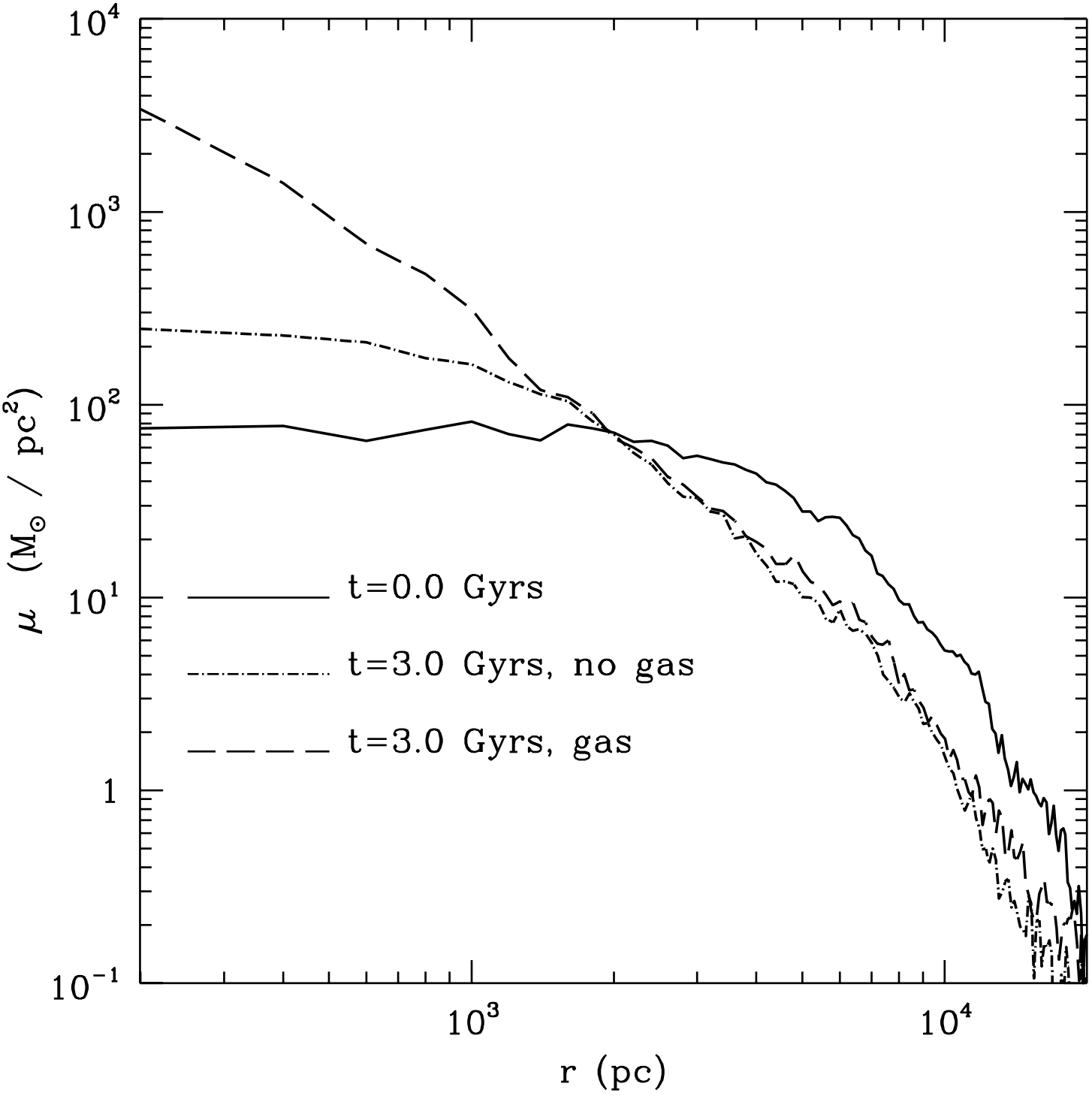
10^4
10^3
10^2
10^1
1
10^{-1}
μ ($M_\odot$ / pc^2)
t=0.0 Gyrs
t=3.0 Gyrs, no gas
t=3.0 Gyrs, gas
10^3
10^4
r (pc)

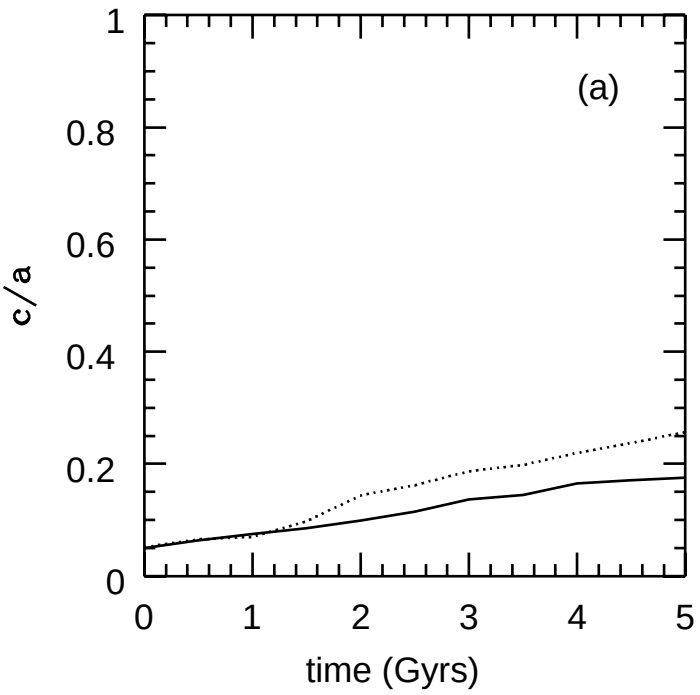
(a)
c/a
time (Gyrs)
0
0.2
0.4
0.6
0.8
1
0
1
2
3
4
5

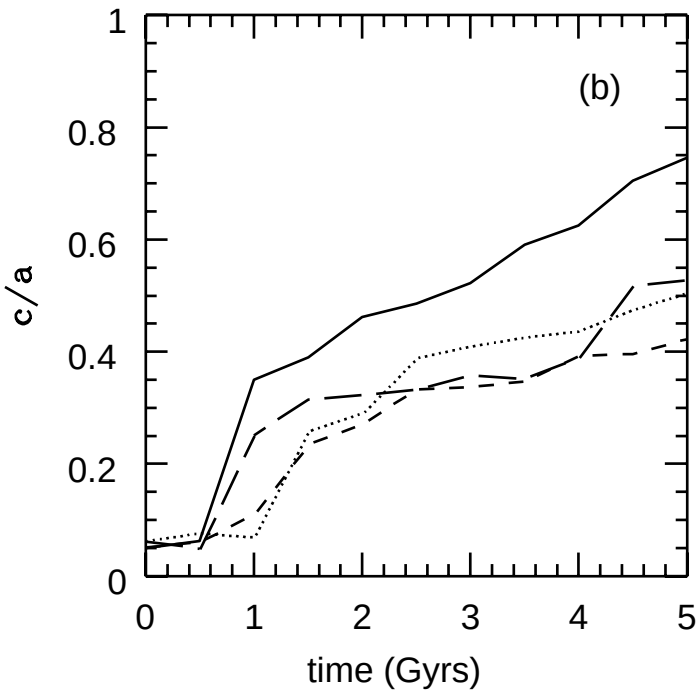
(b)
c/a
time (Gyrs)
0
0.2
0.4
0.6
0.8
1
0
1
2
3
4
5

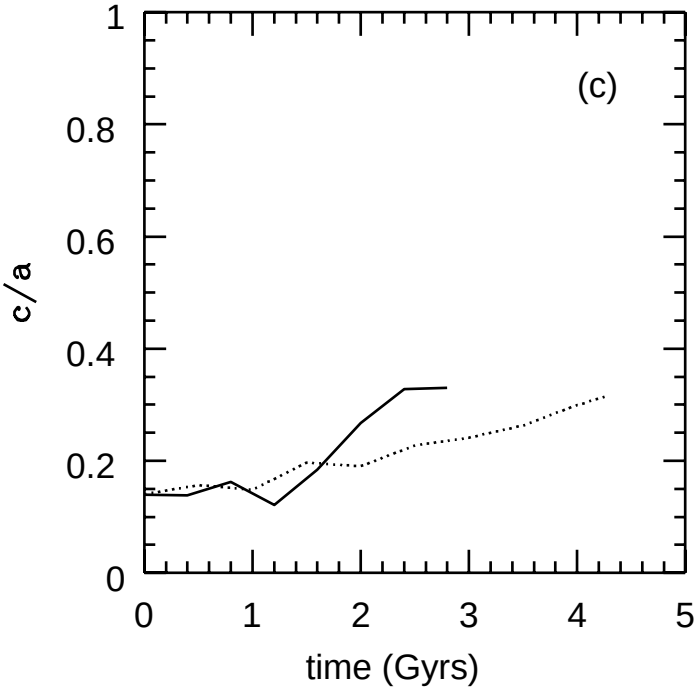
(c)
c/a
time (Gyrs)
0
0.2
0.4
0.6
0.8
1
0
1
2
3
4
5

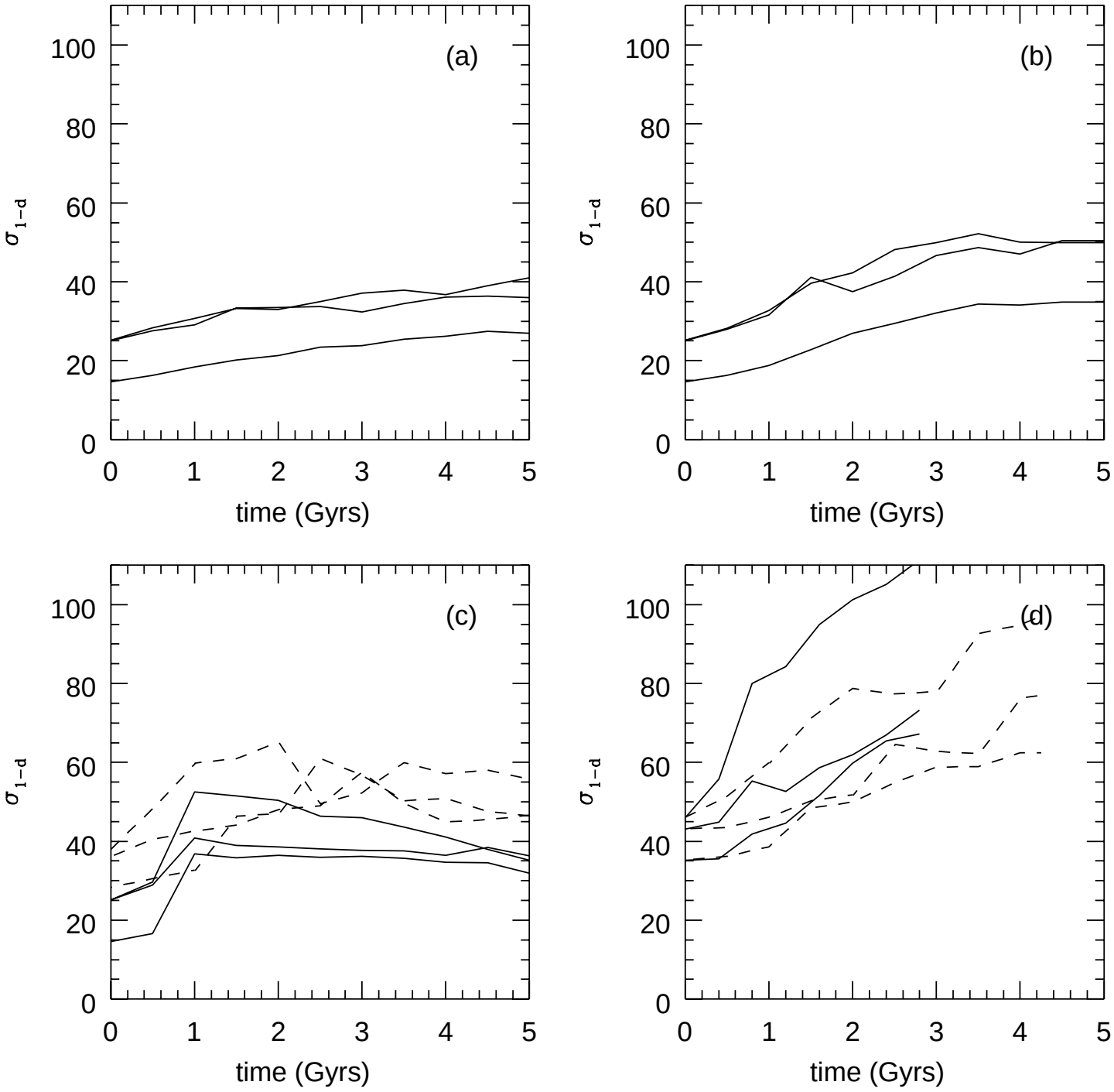
(a)
(b)
(c)
(d)
σ_{1-d}
time (Gyrs)
0
20
40
60
80
100
0
1
2
3
4
5

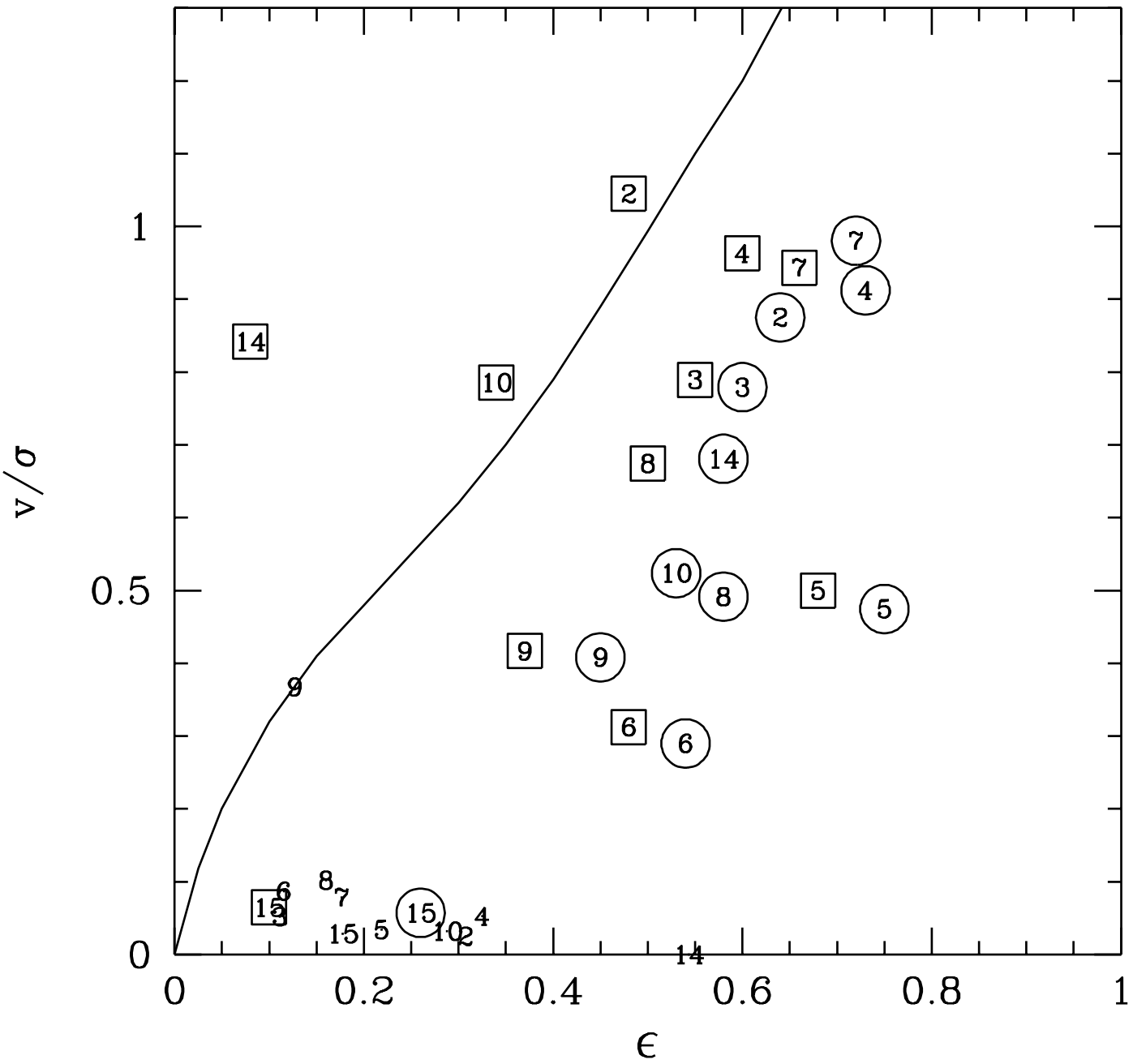
v/σ
ϵ
0
0.5
1
0
0.2
0.4
0.6
0.8
1

Model	Harass	Orbit apo - peri	$M_{*,f}/M_{*,i}$	$M_{*,f}/M_\odot$ r $< r_t$	$M_{d,f}/M_\odot$ r $< r_t$	$M_{T,f}/M_{*,f}$ r $< r_e$	r_t kpc	r_e kpc	μ_e $M_\odot/pc^2$	$\sigma_x, \sigma_y, \sigma_z$ km s^{-1}	v_x, v_y, v_z km s^{-1}	c/a	b/a
ic's	-	-	-	2.0e10	1.1e11	2.70	30	5.3	113	40 40 36	0 0 122	0.10	0.95
1g	no	600-300	0.93	1.8e10	6.4e10	2.17	20	4.0	183	82 82 68	0 0 91	0.19	0.84
2g	yes	450-450	0.82	1.6e10	4.8e10	2.04	16	3.7	188	104 80 67	0 2 70	0.36	0.52
3g	yes	600-300	0.75	1.5e10	3.7e10	1.60	16	3.1	292	117 77 76	2 4 60	0.40	0.45
4	yes	600-300	0.75	1.5e10	3.2e9	1.67	17	3.9	195	80 57 54	1 3 52	0.27	0.40
5	yes	600-300	0.74	1.5e10	2.9e10	1.60	17	3.3	266	98 59 56	0 2 28	0.25	0.32
6	yes	600-300	0.73	1.4e10	2.8e10	1.56	17	2.8	290	96 69 64	3 6 20	0.46	0.52
7	yes	600-300	0.70	1.3e10	3.1e10	1.57	14	3.9	201	81 51 53	3 4 50	0.28	0.34
8	yes	600-300	0.51	1.0e10	1.1e10	1.24	10	2.4	336	75 59 43	0 6 29	0.42	0.50
9	yes	600-300	0.41	8.2e9	7.2e9	1.57	14	2.6	240	59 49 48	9 18 -20	0.55	0.63
10	yes	600-300	0.34	6.8e9	5.1e9	1.47	11	2.5	209	45 63 42	1 2 -33	0.47	0.66
ic's	-	-	-	1.0e10	4.5e10	2.50	22	4.5	60	23 23 15	0 0 87	0.05	0.95
11	no	450-450	0.91	9.5e9	3.8e10	2.40	19	4.8	63	35 36 25	0 0 77	0.13	0.93
12	no	600-300	0.85	8.5e9	2.1e10	2.20	17	4.2	67	49 54 36	0 0 50	0.17	0.85
13	no	600-300	0.82	8.2e9	2.1e10	1.78	13	3.3	113	64 53 45	0 0 30	0.25	0.60
14	yes	600-300	0.56	5.6e9	6.9e9	1.49	9	2.6	127	48 47 38	2 0 32	0.42	0.92
15	yes	600-300	0.27	2.7e9	1.1e9	1.17	6	1.6	161	37 35 31	0 1 -2	0.74	0.90

Table 1. Simulation parameters